JOURNAL OF QUATERNARY SCIENCE (2022) **37**(1) 71–85 ISSN 0267-8179. DOI: 10.1002/jqs.3380

JQS Journal of Quaternary Science QRA Quaternary Research Association

# Insights into Holocene relative sea-level changes in the southern North Sea using an improved microfauna-based transfer function

**JULIANE SCHEDER,[1,2]* FRIEDERIKE BUNGENSTOCK,[2] KRISTIN HAYNERT,[3,4] ANNA PINT,[1] FRANK SCHLÜTZ,[2] PETER FRENZEL,[5] ACHIM WEHRMANN,[3] HELMUT BRÜCKNER[1] and MAX ENGEL[6,7]**

[1]Institute of Geography, University of Cologne, Köln, Germany
[2]Lower Saxony Institute for Historical Coastal Research, Wilhelmshaven, Germany
[3]Marine Research Department, Senckenberg am Meer, Wilhelmshaven, Germany
[4]J.F. Blumenbach Institute of Zoology and Anthropology, Georg August University of Göttingen, Göttingen, Germany
[5]Institute of Geosciences, Friedrich Schiller University Jena, Jena, Germany
[6]Institute of Geography, Heidelberg University, Heidelberg, Germany
[7]Geological Survey of Belgium, Royal Belgian Institute of Natural Sciences, Brussels, Belgium

Received 20 April 2020; Revised 9 September 2021; Accepted 13 September 2021

ABSTRACT: In light of global warming and rising relative sea level (RSL), detailed reconstructions of RSL histories and their controlling processes are essential in order to manage coastal-protection challenges. This study contributes to unravelling Holocene RSL change on the East Frisian North Sea coast in high resolution and with a new approach for the German Bight. For the first time, a transfer function (vertical error: 29.7 cm ≙ ~11% of the mean tidal range) for RSL change based on a combined training set of benthic foraminifers and ostracods from the back-barrier tidal basin of Spiekeroog is applied to the Holocene record of the back-barrier tidal basin of Norderney. The resulting RSL curve for the Norderney tidal basin is corrected for decompaction and shows a deceleration in RSL rise between 6000 and 5000 cal BP. The smallest possible error envelope (~1 m) results from the good suitability of salt-marsh layers between 5000 and 4000 cal BP. The RSL curve provides an approach towards the closure of the common data gap of peat-based curves for the southern North Sea related to a lack of basal peats in the youngest age range, and verifies regional differences in glacial isostatic adjustment. © 2021 The Authors *Journal of Quaternary Science* Published by John Wiley & Sons Ltd.

KEYWORDS: coastal change; Foraminifera; multiproxy approach; northern Germany; Ostracoda

## Introduction

Detailed field-based relative sea-level (RSL) reconstructions are crucial for the understanding of coastal change, for improving glacial isostatic adjustment (GIA) models and for the long-term context of future predictions of RSL rise, which are necessary for coastal-hazard management (Weisse *et al.*, 2012; Woodroffe and Murray-Wallace, 2012; Rahmstorf, 2017). Due to local effects (palaeogeography resulting in flood-basin effects, differences in tidal range, differences in GIA), RSL curves only have local to regional validity (van de Plassche, 1986; Kiden *et al.*, 2002; Bungenstock and Schäfer, 2009; Bungenstock and Weerts, 2012; Meijles *et al.*, 2018). Since existing RSL reconstructions from the southern North Sea region based on basal and intercalated peats (e.g. Behre, 2007; Bungenstock and Schäfer, 2009) depend on the existence of peat beds and often show rather high vertical error ranges of several metres, the necessity of more precise data has been widely expressed (Vink *et al.*, 2007; Bungenstock and Schäfer, 2009; Bungenstock and Weerts, 2010, 2012; Baeteman *et al.*, 2011; Meijles *et al.*, 2018). Therefore, in order to provide more continuous records and thus improve RSL reconstructions, in a first step, a preliminary transfer function (TF) for calculating the indicative meaning of RSL-related data, based on foraminifers and ostracods, was developed for the East Frisian Islands. It provides a vertical error of ±49.1 cm (18.2% of the mean tidal range) (Scheder *et al.*, 2019). Such a TF models the modern relationship between relative species abundances and sample elevations and allows implications on palaeo-water depths with a decimetre-scale precision for mesotidal environments (~10–15% of the tidal range) (Leorri *et al.*, 2010; Kemp *et al.*, 2012; Barlow *et al.*, 2013; Edwards and Wright, 2015). Therefore, it is a direct datum for RSL.

This study presents new foraminifer and ostracod data from a surface transect on the southern coast of the East Frisian Island of Spiekeroog, which are combined with the existing TF data (Scheder *et al.*, 2019) in order to improve the TF performance and reduce the vertical error. The resulting final TF is applied to seven Holocene sediment cores located in the back-barrier area of Norderney (Bittmann, 2019; Bulian *et al.*, 2019). Research hypotheses are:

- The performance of the existing TF can be improved by including additional modern sample data, leading to a smaller vertical error.
- The first ever application of a microfossil-based TF to Holocene sediment cores of the East Frisian North Sea coast leads to an RSL curve with higher resolution than the existing peat-based RSL curves.
- Microfossil-based transfer functions help to better quantify regional differences in GIA and other factors influencing RSL

*Correspondence: J. Scheder, University of Cologne, as above.
E-mail: schederj@uni-koeln.de

in the southern North Sea region by providing a more complete database for RSL curves along the East Frisian coast.

## Study area

The East Frisian barrier islands are situated in the southern North Sea, off the coast of north-western Germany; they have formed since the deceleration of the post-glacial sea-level rise around 7.5–6 ka ago (Freund and Streif, 2000; Flemming, 2002; Vink *et al.*, 2007). Their south-eastward shift of several kilometres since then is driven by the ongoing RSL rise and prevailing longshore current (Streif, 1990; Flemming, 2002). Long-term tectonic movements can be roughly estimated from the depth of submerged Eemian sea-level highstand data (e.g. Kiden *et al.*, 2002; Streif, 2004; Vink *et al.*, 2007). Vink *et al.*, 2007 translate the ages and depths of said deposits to linear tectonic uplift rates of 0.04–0.16 m/ka along the East Frisian Islands for the Holocene. The two study areas (Fig. 1a) investigated here are the tidal basins of the islands of Spiekeroog (Fig. 1b–d) and Norderney (Fig. 1e,f). Spiekeroog is limited by the tidal inlets Otzumer Balje in the west and Harle in the east, channelling water of semi-diurnal tides with a mean tidal range of 2.7 m (BSH, 2018). Norderney is situated between the tidal inlets Norderneyer Seegat in the west and Wichter Ee in the east with a mean tidal range of 2.5 m (BSH, 2018). Both islands are characterised by intertidal back-barrier tidal flats, which transform into supratidal salt marshes onshore. A humid temperate climate (Cfb after the Köppen-Geiger classification) prevails in the complete area (Kottek *et al.*, 2006; Beck *et al.*, 2018).

The investigated transect of surface sediment samples (*c.* 230 m in a north–south direction, *c.* 180 m west of the transect by Scheder *et al.*, 2019) covers the natural salt marsh and *c.* 100 m of the adjacent tidal flat (Fig. 1b–d) and complements the transect by Scheder *et al.* (2019). The natural salt marsh in the back-barrier of Spiekeroog consists of the upper salt marsh and the lower salt marsh, based on different shore height, inundation frequency and hydro-morphological parameters (van Wijnen and Bakker, 2001). The lower salt marsh is dominated by *Elytrigia atherica*, *Puccinellia maritima* and *Atriplex portulacoides*. Halophytic plants such as *Salicornia* spp. and *Spartina anglica* predominantly colonise the pioneer zone (Bakker, 2014). In contrast to the salt marsh, the adjacent tidal flat is characterised by marine resources such as marine detritus, micro- and macrophytobenthos (Flemming *et al.*, 1994; Flemming and Ziegler, 1995).

The investigated sediment cores are located along a transect (*c.* 7000 m in an overall east–west direction) in the back-barrier tidal flat of Norderney, starting in the west at the inner margin of the tidal inlet 'Norderneyer Seegatt', reaching to the east across the sand flat 'Hohes Riff', where they cross a smaller tidal channel.

## Methods

### Fieldwork

#### Modern samples

The surface samples (0–1 cm) in addition to those in Scheder *et al.* (2019) were collected as part of an independent study along 11 transect stations from the salt marsh (stations 1–8) to the tidal flat (stations 9–11) using a soil corer (Ø 10 cm). Due to small-scale patchiness, three replicates were taken at each transect station resulting in 33 samples. The sediment samples were transferred into Kautex wide-neck containers, preserved with Rose Bengal ethanol (94%) solution (2 g/l) to stain the protoplasm in all living foraminifers and to differentiate between living specimens and dead/empty tests as described by Walton (1952), Lutze and Altenbach (1991) and Edwards and Wright (2015). The samples were stored for three weeks until further processing in the laboratory. For biochemical analysis, data for oxygen and TOC (total organic carbon) were measured at each transect station. Replicates (3n) of oxygen were determined with a Fibox 4 oxygen meter (PreSens – Precision Sensing GmbH) in the surface sediment from 0 to 1 cm. Additional samples for TOC analysis were taken from the surface sediment (<2 cm) and frozen at -20°C until measurement. The elevation of the 11 transect stations related to NHN (*Normalhöhennull* = German standard elevation) was determined using a differential GPS (DGNSS Stonex S9) with real-time correction service. The applied sampling method only slightly differs from that of the existing dataset (Scheder *et al.*, 2019); in particular, concerning the sample thickness (3 cm for existing dataset, 1 cm for additional samples). However, due to negligible variability of species associations within the upper 3 cm (Scheder *et al.*, 2019), the results are expected to be comparable. The data of both independent studies were merged in a later step.

#### Core drillings

On the tidal flats, cores were retrieved using a vibrocorer (Wacker Neuson IE high-frequency vibrator head and generator) and aluminium tubes (8 cm diameter, 6 m length), whereas tidal-channel cores were drilled from the research vessel *MS BURCHANA* using a vibrocorer VKG-6 (VC-6000, med consultans GmbH) and plastic liners (10 cm diameter, 5 m length). Opening and macroscopic core description after Preuß *et al.* (1991) was conducted either at the Lower Saxony Institute for Historical Coastal Research (Wilhelmshaven, Germany) or the Institute of Geography of the University of Bremen (Germany). Sampling mainly followed 10 or 20 cm intervals with additional samples in smaller-scale layers of interest.

Additional information for correlation was taken from archive core data provided by the 'Landesamt für Bergbau, Energie und Geologie' (LBEG, Hannover, Germany).

### Laboratory analyses

#### Modern surface samples

Samples were washed with tap water and first passed through a 2000 µm screen, in order to remove macrophyto- and macrozoobenthos. Subsequently, the samples were washed through a 63 µm sieve and dried at 60°C for at least 24 h. The >63 µm fraction was split by using a microsplitter and analysed for living and dead individuals. Living individuals (=with Rose Bengal-stained protoplasm and preserved soft parts in ostracods) and dead/empty tests (=without stained protoplasm and empty ostracod valves) were picked, sorted by species and counted under a stereo microscope (Leica MZ12). Tests were mounted in Plummer cell slides with glue (Rahman, 2018) and ostracod valves were stored in Fema cells. Determination of foraminifer species followed the descriptions in Frenzel *et al.* (2005), Müller-Navarra *et al.* (2016) and the foraminifera.eu database (Hesemann, 2015), whereas ostracod taxa were determined based on Athersuch *et al.* (1989) and Frenzel *et al.* (2010).

TOC samples were measured using the CHNS elemental analyser 'vario EL cube' (Elementar Analysensysteme GmbH). Prior to analysis, carbonates were removed by treatment with HCl (10%). The precision of the measurement was <0.2% (for a detailed description, see Lange *et al.*, 2018).

 

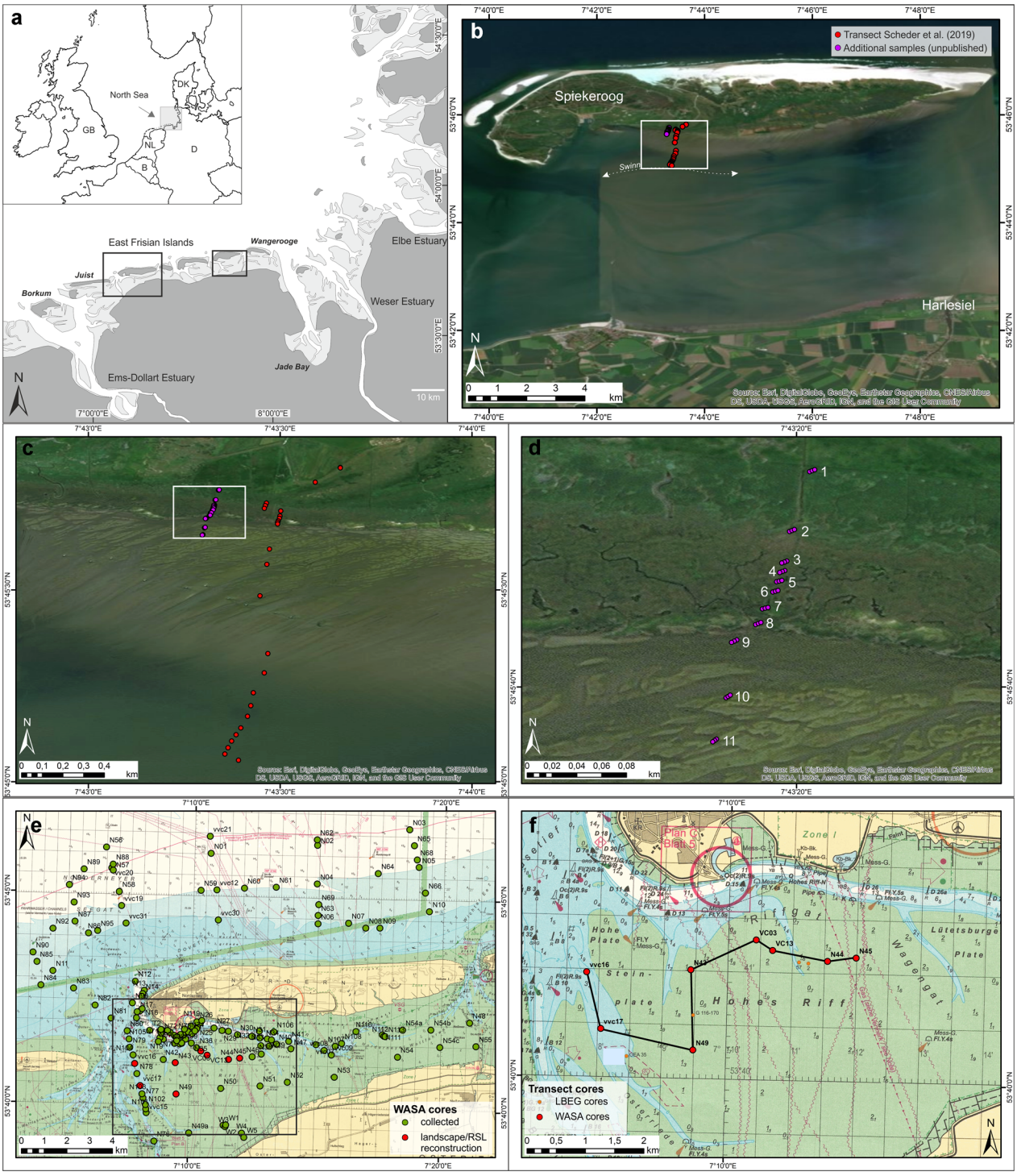


**Figure 1.** Study area. a: overview map of the North Sea with Spiekeroog and Norderney framed; b: overview of Spiekeroog with the transect investigated by Scheder *et al.* (2019) and the additional transect of modern microfauna; c: detail image showing the location of both transects in the salt marsh and tidal flat; d: detail of the additional transect; e: overview of Norderney with all WASA cores (cores for TF application are marked in red); f: detail of the cores used for TF application and RSL reconstruction. WASA = *The Wadden Sea as an archive of landscape evolution, climate change and settlement history*. Map sources: b–d: Esri, Digital Globe, GeoEye, Earthstar Geographics, CNES/Airbus DS, USDA, USGS, Aerogrid, IGN, and the GIS User Community; e–f: Bundesamt für Seeschifffahrt und Hydrographie, 2016. [Color figure can be viewed at wileyonlinelibrary.com]

*Core samples*

Microfaunal, sedimentological and geochemical investigations were performed for 137 samples from seven sediment cores (for details see S1.1 (suppl.)) for facies interpretation (see also Elschner *et al.*, 2021). Core VVC17 was analysed as described in Bulian *et al.* (2019).

The chronological framework is based on AMS-$^{14}$C dating on peats (Bulian *et al.*, 2019), *in-situ* bivalves and foraminifer tests. $^{14}$C dating was performed by the Poznan Radiocarbon Laboratory (Poland) and Beta Analytic Inc. (USA). Calibration and age–depth modelling was accomplished using R software (rbacon, v. 2.3.9.1, Blaauw and Christen, 2019), calibration curves IntCal13 and Marine13 (Reimer *et al.*, 2013) and reservoir correction after Enters *et al.* (2021), who dated two bivalves (*Cerastoderma edule* and *Mytilus edulis*) which were collected near Wangerooge in 1889 (Table 1). The available age data were used by R to interpolate an age model up until the surface, where necessary layer boundaries were integrated in the modelling

 

**Table 1.** AMS $^{14}$C data chart.

| Core | Depth (m NHN) | Lab. code | Dated material | Conventional $^{14}$C age & uncertainty ($^{14}$C a BP) | Calibration | | Calibrated age, 95% probability (cal BP) |
|---|---|---|---|---|---|---|---|
| | | | | | Dataset[1] | Delta R[2] | |
| VVC16 | −5.65 | Poz-94979 | fine bulk | 5600 ± 40 | 1 | | 6453–6299 |
| | −5.80 | Poz-94630 | *Carex, Hydrocotyle* | 5850 ± 35 | 1 | | 6745–6561 |
| | −5.975 | Poz-94641 | charred Ericaceae | 6140 ± 40 | 1 | | 7163–6930 |
| | −6.31 | Poz-94642 | charred grasses | 5190 ± 40 | 1 | | 6171–5773 |
| | −6.52 | Poz-94976 | fine bulk | 5515 ± 35 | 1 | | 6399–6223 |
| | −6.52 | Poz-94631 | *Cladium mariscus* | 5350 ± 35 | 1 | | 6271–6002 |
| | −6.72 | Poz-94633 | *Carex, Hydrocotyle, Ranunculus repens* | 5870 ± 35 | 1 | | 6783–6569 |
| | −6.72 | Poz-94634 | charred Ericaceae and grasses | 5930 ± 35 | 1 | | 6850–6667 |
| | −6.9 | Poz-94978 | fine bulk | 7000 ± 50 | 1 | | 7938–7712 |
| | −6.9 | Poz-94643 | charred Ericaceae and grasses | 7080 ± 50 | 1 | | 8000–7796 |
| VVC17 | −4.82 | Poz-94535 | *Cladium mariscus, Carex flava*-type | 4690 ± 40 | 1 | | 5480–5320 |
| | −4.82 | Poz-95124 | fine bulk | 4780 ± 40 | 1 | | 5600–5460 |
| | −5.45 | Poz-95026 | fine bulk | 5100 ± 40 | 1 | | 5920–5750 |
| | −6.235 | Poz-94532 | *Cladium mariscus* | 5320 ± 40 | 1 | | 6210–5990 |
| | −6.525 | Poz-94533 | fine bulk | 6050 ± 40 | 1 | | 7000–6790 |
| | −6.575 | Poz-94534 | fine bulk | 6710 ± 40 | 1 | | 7700–7510 |
| N49 | −1.18 | Poz-120122 | *Ammonia* group | 4200 ± 70 | 2 | 74 ± 16 | 4393–3978 |
| | −1.95 | Beta-554300 | *Ammonia* group | 3370 ± 30 | 2 | 74 ± 16 | 3243–3005 |
| | −2.97 | Poz-120123 | *Ammonia* group | 3030 ± 120 | 2 | 74 ± 16 | 3005–2365 |
| | −2.99 | Poz-97990 | *Barnea candida* (in living position) | 1350 ± 30 | 2 | 74 ± 16 | 905–733 |
| | −3.07 | Poz-106641 | fine bulk | 3940 ± 35 | 1 | | 4515–4255 |
| | −3.29 | Poz-115426 | fine bulk | 4645 ± 30 | 1 | | 5465–5311 |
| | −3.29 | Poz-115164 | *Phragmites australis* | 3795 ± 35 | 1 | | 4346–4010 |
| | −4.27 | Poz-106643 | stem, rhizome | 4205 ± 30 | 1 | | 4845–4628 |
| N43 | −0.8 | Poz-120120 | *Ammonia* group | 5590 ± 40 | 2 | 74 ± 16 | 5995–5755 |
| | −0.8 | Poz-120121 | *Haynesina germanica* | 2810 ± 50 | 2 | 74 ± 16 | 2650–2324 |
| | −2.775 | Poz-106624 | charred plant remains | 3385 ± 35 | 1 | | 3717–3515 |
| | −4.625 | Poz-106640 | *Cladium mariscus* | 4470 ± 35 | 1 | | 5289–4974 |
| VC03 | −2.7 | Poz-93522 | *Cerastoderma edule* (articulated) | 630 ± 30 | 2 | 74 ± 16 | 278–78 |
| | −3.085 | Poz-95925 | *Cerastoderma edule* (articulated) | 600 ± 30 | 2 | 74 ± 16 | 260–1 |
| | −3.64 | Poz-116736 | charred stem remains (Poaceae) | 4235 ± 35 | 1 | | 4863–4645 |
| VC13 | −1.415 | Poz-120125 | *Ammonia* group | 5320 ± 60 | 2 | 74 ± 16 | 5741–5462 |
| | −1.55 | Poz-93524 | *Mya arenaria* (in living position) | 127.84 ± 0.38* | 2 | 74 ± 16 | 1598–584 |
| | −2.335 | Beta-554302 | *Ammonia* group | 4030 ± 30 | 2 | 74 ± 16 | 4065–3841 |
| | −2.725 | Poz-120126 | *Ammonia* group | 2890 ± 50 | 2 | 74 ± 16 | 2711–2390 |
| | −2.735 | Poz-93523 | *Mytilus edulis* | 560 ± 30 | 2 | 74 ± 16 | 228–1 |
| | −2.93 | Poz-115133 | fine bulk | 3660 ± 30 | 1 | | 4084–3899 |
| | −3.72 | Poz-115134 | *Cladium mariscus* | 4100 ± 35 | 1 | | 4814–4449 |
| N44 | −2.915 | Poz-115136 | *Phragmites australis* | 3330 ± 30 | 1 | | 3637–3477 |
| | −2.915 | Poz-115163 | charred stem remains | 3335 ± 35 | 1 | | 3682–3475 |
| | −3.185 | Poz-112307 | *Schoenoplectus, Potentilla anserina* | 3580 ± 35 | 1 | | 3980–3729 |

[1]1: IntCal13 (for northern hemisphere terrestrial $^{14}$C dates); 2: Marine13 (for marine $^{14}$C dates).
[2]Delta R value and uncertainty used for reservoir correction of marine $^{14}$C dates after Enters *et al.* (2021).
*pMC modern; dated botanical plant material are seeds and fruits from identified taxa, for Ericaceae twigs and leaves, vegetative remains of *Phragmites* or unclear identity.

process in order to account for different possible sedimentation rates.

### Data analysis

In order to analyse the influence of elevation, oxygen and TOC on the abundance of intertidal foraminifers, a redundancy analysis (RDA) was performed using the software CANOCO 5 (Microcomputer Power, Ithaca, USA, 2012). Microfaunal data of the preliminary TF (Scheder *et al.*, 2019) were combined with the additional foraminifer and ostracod data (dead assemblages). All measured elevations were transformed to the most recent vertical datum (DHHN2016; '*Deutsches Haupthöhennetz*'). Pearson and Spearman correlation coefficients were calculated showing no auto-correlations between taxa. In order to verify elevation, connected to the inundation frequency, as the main driving factor of species composition and that the unimodal response along the main environmental gradient does not change after adding the new samples, principal component analysis (PCA) and detrended correspondence analysis (DCA) were performed. Correlation and multivariate statistics were accomplished using the software PAST (v.3.2.1) (Hammer *et al.*, 2001). The gradient length indicated by the DCA (3.86 standard deviation (SD)) suggests a more unimodal species–environment relationship (Birks, 1995; Lepš and Šmilauer, 2003). Therefore, the final TF was modelled using the weighted averaging–partial least squares (WA-PLS) method. The choice of a multicomponent model was not only based on the coefficient of determination ($R^2_{boot}$) and the root mean square error of prediction (RMSEP) (cf. Wright *et al.*, 2011), but also on considerations in Barlow *et al.* (2013). In their case, two- or three-component models provide a better statistical fit across the elevation range of the modern training set. Furthermore, variables also affecting microfaunal distributions show covariations with the elevation. They state that multiple-component models are acceptable due to the statistical structure of residuals of a one-component model reflecting these relationships. Hence, we applied a WA-PLS model with a maximum of three components, in order to avoid overfitting (Kemp and Telford, 2015) using the software C2 (v. 1.7.7) (Juggins, 2007). The TF performance was evaluated by bootstrapping cross-validation (1000 cycles) based on the $R^2_{boot}$, estimating the quality of the linear relationship between observed and estimated elevations, and the RMSEP, facilitating the assessment of the general predictive capability of the TF (Milker *et al.*, 2017). The appropriate component was chosen based on the lowest RMSEP and highest $R^2_{boot}$.

Core data were processed and evaluated similarly to the modern dataset (Scheder *et al.*, 2019) (for more detail, see S1.2 (suppl.)). Where possible, facies identified from the cores were correlated in a cross section, in order to get an understanding of their spatial extent. Only supratidal and intertidal layers, identified based on the core investigations, were used for the application of the TF, since the TF is only able to reconstruct these depositional environments. The quality of the reconstruction was evaluated by the modern analogue technique (MAT) based on the minimum dissimilarity coefficient (MinDC) using the software C2 and following suggestions by Watcham *et al.* (2013), who separate fossil samples into good (<5%), close (<20%) and poor (>20%) modern analogues.

### Decompaction and 2σ uncertainty

Post-depositional and auto-compaction of peat can lead to significant uncertainties when reconstructing past sea levels (Bird *et al.*, 2004; Long *et al.*, 2006; Hijma *et al.*, 2015). For instance, auto-compaction by oxidation and decomposition can cause surface subsidence of several metres over millennial timescales (e.g. Long *et al.*, 2006; Weerts, 2013). In our case, peats are not used to reconstruct the RSL but their compaction as well as the compaction of mud-rich sediments can influence the elevation of the used sediment samples, so a decompaction approach is required.

For decompaction of our TF samples from the minerogenic salt-marsh area we applied a factor of 1.5 for the sediment thickness underneath the sample down to the Holocene base, where this is known, assuming that the underlying coarse-grained Pleistocene sediments are compaction-free. We refer to values from literature, e.g. Pizzuto and Schwendt (1997), who use a numerical model to quantify auto-compaction in valley-fill deposits. They study cores with less than 10 m length in organic-rich mud (salt marsh) and siliciclastic mud (subtidal). They calculate a factor of 2.2 (54% compaction) for organic-rich mud and 1.3 (23% compaction) for the entire core section. Van Asselen (2011) considers a decompaction factor for peat of 1.7 (40% compaction) with an average factor of 1.8 (~45% compaction) for basal peat and 1.3–1.5 (~20–30% compaction) for intercalated peat. Smith *et al.* (2003) use values between 1.7 (40% compaction) and 3.1 (68% compaction) for peat overlain by clastic sediments. If the clastic unit is >2.5 m thick, they assume that the compaction of the underlying peat is complete before the respective sample material deposited. Therefore, we assume that the presence of basal peat does not change the downcore correction factor of 1.5 for the TF samples, because its main compaction was completed before the overlying salt-marsh sequence formed.

For the basal peats, we apply a different decompaction factor, as we expect a much stronger compaction by oxidation and decomposition and later additional compression by overlying clastic deposits. Here, we apply a decompaction factor of 2.5 (e.g. van de Plassche *et al.*, 2005, 2010; Hijma *et al.*, 2015; Khan *et al.*, 2019).

The 2σ vertical uncertainty of the samples, including their sample-specific error calculated by the TF, was determined applying the standardised calculation of the indicative meaning following the HOLSEA concept (Khan *et al.*, 2019) (supplementary excel file).

## Results of the modern samples

Back-barrier foraminifers from the second transect of Spiekeroog (violet transect in Fig. 1c and d) follow a typical horizontal zonation (Table S2.1 (suppl.)). Accordingly, agglutinated species (*Deuterammina balkwilli* (Brönnimann & Whittaker, 1983), *Jadammina macrescens*, as a synonym for *Entzia macrescens* (Brady, 1870), *Miliammina fusca* (Brady, 1870), *Trochammina inflata* (Montagu, 1808)) and miliolid calcareous species (*Cornuspira involvens* (Reuss, 1850) and *Triloculina oblonga* (Montagu, 1803)) tend to have a higher abundance in vegetated supratidal and intertidal environments with higher elevation (salt marsh, transect stations 1 to 8, +1.946 to +0.808 m NHN; Fig. 2). In comparison, hyaline calcareous species (*Ammonia tepida* (Cushman, 1926), *Haynesina germanica* (Ehrenberg, 1840), *Elphidium* spp. (Montfor, 1808)) occur with higher abundances in lower intertidal and subtidal elevations (tidal flat, transect stations 9 to 11, +0.683 to +0.926 m NHN; Fig. 2). Ostracods follow the same zonation but exhibit a transition zone between the vegetated salt marsh and the lower elevations of the tidal flat. The vegetated salt marsh and most of the pioneer zone are almost exclusively characterised by high abundances of *Leptocythere* (Sars, 1925), especially *L. lacertosa* (Hirschmann, 1912). The transition zone between the pioneer zone and the tidal flat shows the highest abundances (mainly

 

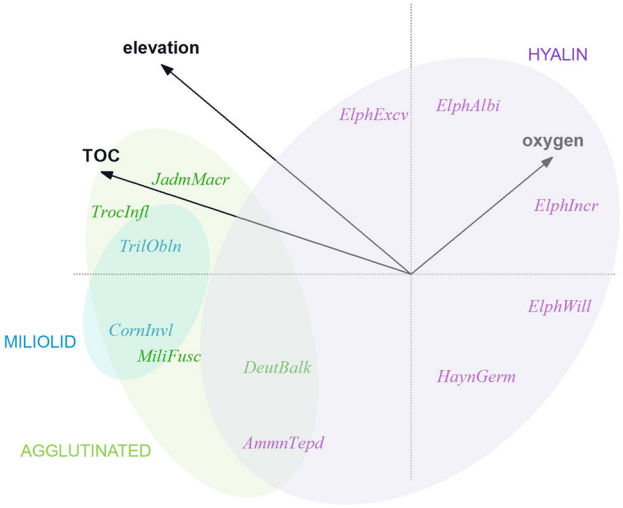


**Figure 2.** Redundancy analysis of supratidal to intertidal foraminifers in relation to elevation, oxygen and total organic carbon. Eigenvalues of axis 1 = 0.3932 and axis 2 = 0.0806. Full species names of agglutinated species: *DeutBalk* = *Deuterammina balkwilli*, *JadmMacr* = *Jadammina macrescens* (= *Entzia macrescens*), *MiliFusc* = *Miliammina fusca*, *TrocInfl* = *Trochammina inflata;* miliolid species: *CornInvl* = *Cornuspira involvens*, *TrilObln* = *Triloculina oblonga;* hyaline species: *AmmnTepd* = *Ammonia tepida*, *HaynGerm* = *Haynesina germanica*, *ElphAlbi*, *ElphExc*, *ElphIncr*, *ElphWill* = *Elphidium* spp. (*E. albiumbilicatum, E. excavatum, E. incertum, E. williamsoni* (as synonym for *Cribroelphidium williamsoni*)). [Color figure can be viewed at wileyonlinelibrary.com]

*Leptocythere* and *Cytherois fischeri* (Sars, 1866)) and the tidal flat shows additional *Semicytherura striata* (Sars, 1866).

Environmental parameters such as oxygen concentration and TOC play a major role in the distribution of foraminifers. Along the transect, the mean oxygen concentration increases from 178.3 ± 27.79 µmol/l in the upper salt marsh to 229.9 ± 58.07 µmol/l in the lower salt marsh and 224.1 ± 54.84 µmol/l in the tidal flat, whereas the TOC content decreases from 6.1 ± 0.95% to 3.2 ± 1.92% and 0.3 ± 0.10%, respectively (Tables S2.2 and S2.3 (suppl.)). Accordingly, the abundance of agglutinated and miliolid species correlates with higher TOC in vegetated intertidal environments and is less impacted by oxygen (Fig. 2). In contrast to that, the abundance of hyaline species correlates with oxygen in subtidal elevations and is less impacted by TOC (Fig. 2). RDA suggests a correlation between TOC and elevation (Fig. 2). This is in accordance with the previous study of Scheder *et al.* (2019), which reveals a high Pearson correlation coefficient of ~0.75.

## Results and interpretation of the statistical analyses

### *The combined modern training set*

In order to cover information over longer time periods and avoid seasonal influences, only the dead assemblages were used for combining the modern data of this study with the data from Scheder *et al.* (2019), since those average the result of habitat preferences and related taphonomic changes over several seasons and years (Murray, 2000).

After comparing the new samples with the previous samples of the preliminary TF (Scheder *et al.*, 2019), the rare foraminifer previously determined as *Spirillina* sp. could be re-identified as *Cornuspira involvens* (Reuss, 1850) based on the identification of the additional modern samples. Identification of the other taxa remains unchanged. In the combined dataset, both Pearson and Spearman correlation show no (auto-)correlations between foraminifer and ostracod taxa. Thus, all taxa were included in the following PCA. This was performed in order to find variables accounting for as much of the variance in the combined dataset as possible (Davis, 1986; Harper, 1999) using samples with a minimum of 40 individuals. This limit was defined in order to find a balance between high accuracy of reconstructed data points (higher number of individuals) and a higher quantity of data points (lower number of individuals). The PCA (Fig. 3) reveals two components with variances >10%.

The most significant axis is PC 1 (31.99%), opposing salt-marsh foraminifers and associated samples (positive values) and shallow-water, i.e. intertidal, species and associated tidal-flat samples (negative values) suggesting a salt-marsh vs. tidal-flat component. This could be related to salinity, organic content and hydro-dynamic levels, which are all controlled by the duration of water cover or inundation frequency (Scheder *et al.*, 2019). PC 1 is therefore interpreted to represent the elevation, meaning that the combined dataset can be used for the development of the final TF.

PC 2 (17.61%) opposes euryhaline species with tolerances towards dysoxic conditions (e.g. *Ammonia tepida*) (negative values) and species less tolerant of dysoxic conditions (e.g. *Trochammina inflata*) (positive values) (Murray, 2006). Dysoxic conditions may relate to finer-grained substrates, whereas oxic conditions are associated with sand-dominated substrates. PC 2 may therefore relate to the oxygen availability or the substrate.

The DCA was carried out in order to test the species–environment relationship including the elevation and the microfaunal data. The length of the environmental gradient was determined as 3.86 SD suggesting a more unimodal species–environment relationship (Birks, 1995; Lepš and Šmilauer, 2003).

### *Final transfer function*

As performed for the preliminary TF (Scheder *et al.*, 2019), two models were developed (Fig. 4): Model I exclusively

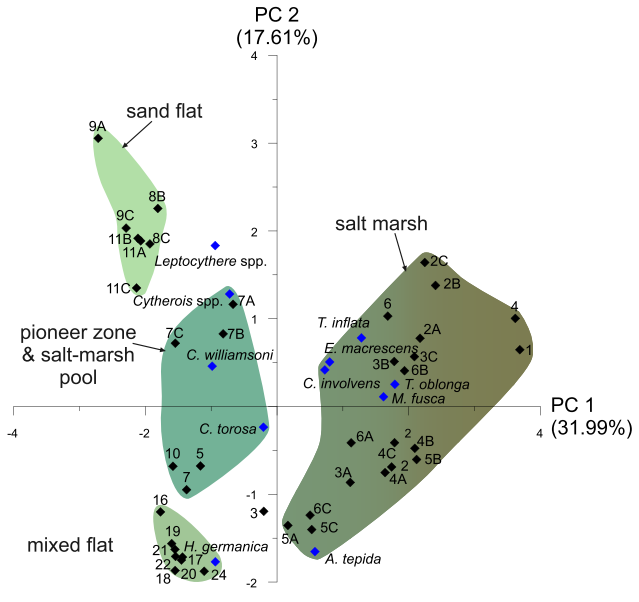


**Figure 3.** Principal component analysis (PCA) biplot showing the two most relevant axes. Black diamonds represent samples, blue diamonds represent foraminifer and ostracod taxa. Colour shades correspond to facies colours used also for core drawings (Figs. S2.3–S2.9 (suppl.)) and for the stratigraphic cross section (Fig. 5). [Color figure can be viewed at wileyonlinelibrary.com]

considers foraminifers (commonly applied approach) and Model II additionally considers the ostracods. For both, the third of the three modelled components is the most suitable (lowest RMSEP and highest $R^2$). During initial modelling, sample 1 A (highest elevation) was identified as an outlier based on visual evaluation of the cross-validation diagrams. It was therefore excluded from the dataset, resulting in an elevation gradient of ~2.71 m in vertical distance (+1.506 to -1.206 m NHN). This is comparable to the mean tidal range of Spiekeroog (2.7 m) with mean high water at +1.4 m NHN and mean low water at -1.3 m NHN (BSH, 2018).

Model I shows an $R^2_{boot}$ of 0.81 and an RMSEP of 37.8 cm, which accounts for 13.92% of the elevation gradient (13.98% of the mean tidal range). No clear trend in the TF over- or underestimating samples related to their observed elevation is visible and no structures of residuals can be documented (Fig. 4). However, underestimation seems to be higher than overestimation.

Model II delivers an $R^2_{boot}$ of 0.89 and an RMSEP of only 29.7 cm, accounting for 10.98% of the elevation gradient (11.02% of the mean tidal range). The residuals show reduced underestimation compared with Model I, indicating an improved precision (Fig. 4).

There is remaining potential to further improve the TF by applying Bayesian modelling, which would consider additional proxies and multimodal species response to the environmental variable (Cahill *et al.*, 2016). However, due to the unimodal species response in the current dataset, this was not implemented here.

## Results and interpretation of the Holocene sediment cores

The facies of the investigated sediment cores are depicted along a west–east transect, which also includes information from four archive cores (Fig. 5). For detailed sedimentological, geochemical and microfaunal results of the investigated cores, see Figs. S2.2–S2.8 (suppl.; for VVC17 see Bulian *et al.*, 2019). Detailed information on $^{14}C$ dating is given in Table 1.

The investigated sedimentary record in the study area starts with Eemian marine highstand sediments documented in the

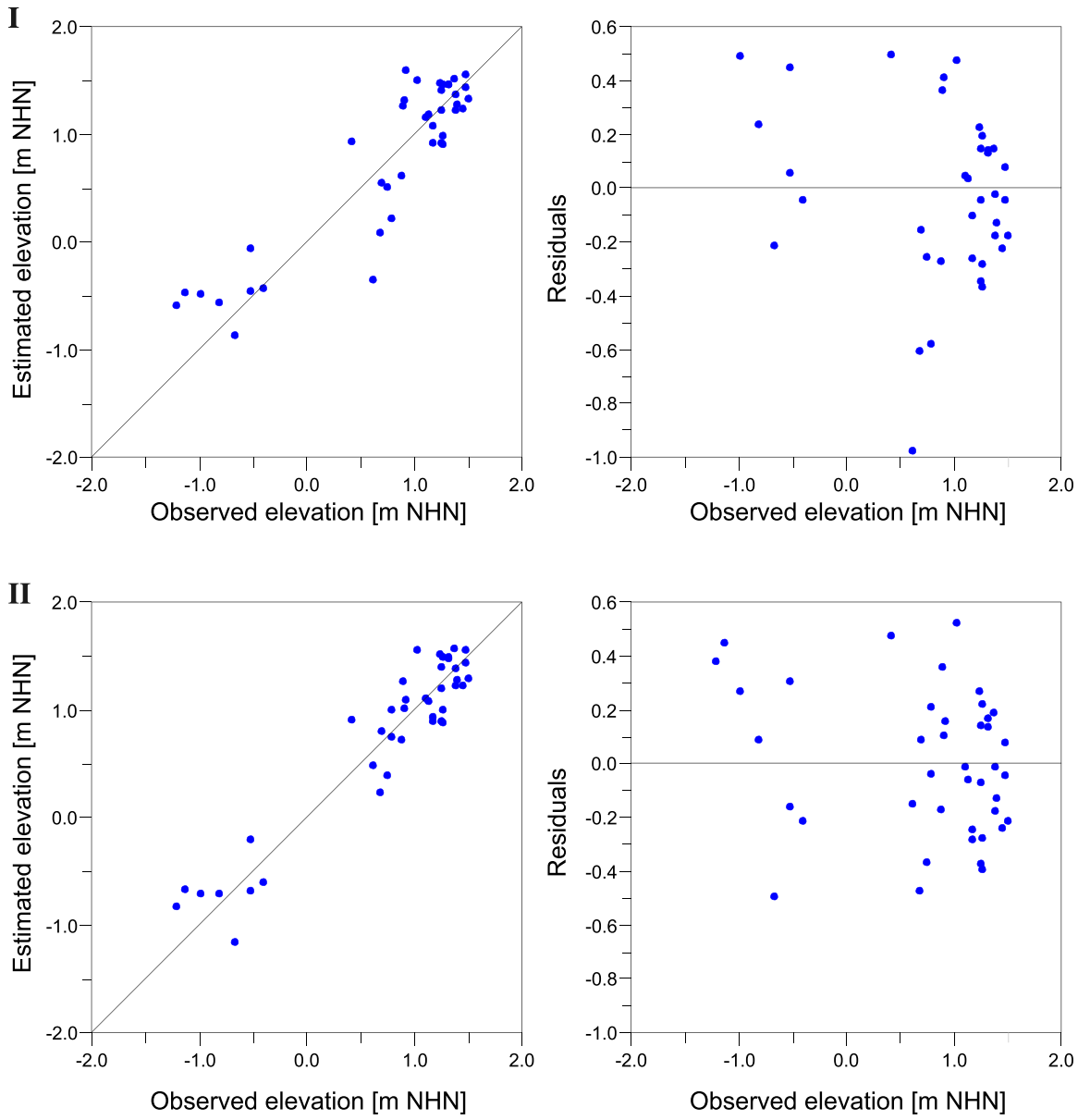


**Figure 4.** Testing of the transfer function by bootstrapping cross-validation (1000 cycles). Diagrams show estimated vs. observed elevation (left) and deviation of samples from the observed elevation (right) for both Model I (dead foraminifers) and Model II (combined associations of dead foraminifers and ostracods). [Color figure can be viewed at wileyonlinelibrary.com]

most western core (VVC16). During the following Weichselian glaciation, the area was subject to periglacial conditions and the accumulation of aeolian and glacio-fluvial sands (Streif, 2004), showing initial pedogenesis (palaeosol in Fig. 5). The upper boundary of these deposits marks the Holocene base, which in the eastern part was reconstructed based on depth information from archive core data.

Around 8–7 ka cal BP, a basal peat started to develop first in the west (VVC16 and 17), driven by rising groundwater levels and the tidal-channel situation during the post-glacial transgression (Bungenstock and Schäfer, 2009). In the east (N43, VC03, VC13, N44–45), the basal peat formed later due to the higher topography. The area slowly started to become protected by early barrier-island formation, which was initiated during the deceleration of sea-level rise around 7–6 ka ago (Freund and Streif, 2000; Flemming, 2002; Bungenstock and Schäfer, 2009).

When sea level had almost reached the position of VVC16 (-6.52 m NHN) and VVC17 (~-6.24 m NHN) around 6000 cal BP, a salt marsh formed, enabling the settlement of typical salt-marsh foraminifers (e.g. *Entzia macrescens* and *Trochammina inflata*) and salt-tolerant plants, indicated by higher organic contents and low C/N ratios (Last and Smol, 2001).

In VVC17, after the salt-marsh phase, peat growth continued simultaneously with basal peat formation in the eastern part, indicating that the peat of that age and depth (-5.47 m NHN in VVC17) is related to sea level due to the formation of basal peats at or above mean sea level. The intercalated salt-marsh deposits probably accumulated due to the ingressing sea along the main channels. This caused regular flooding of the basal peat (VVC17) and subsequent salt-marsh formation. Based on the high sediment supply in the vicinity of the tidal channels and following vertical growth, finally, peat was able to re-establish (intercalated peat in VVC17) (cf. Baeteman, 1999). N49 shows another similar intercalated peat at -3 m NHN, which has an upper erosional contact and is not documented in the other cores. The peat could have formed locally, explaining its absence in the adjacent cores. However, the erosional contacts described in N43, VC03 and VC13 may indicate that this peat has been eroded in these cores. Furthermore, LBEG maps ('Profiltypenkarte', 'NIBIS® Kartenserver', https://nibis.lbeg.de/cardomap3/) show intercalated peats in this area, which is why a more extensive peat formation and subsequent erosion is more likely. $^{14}$C dating of the intercalated peat in N49 shows age inversions. The base was dated to 5465–5311 cal BP (bulk sample; -3.29 m NHN), being older than the basal peat of this core (4845–4628 cal BP; -4.27 m NHN). A second sample at the same depth was dated to 4346–4010 cal BP (*Phragmites australis*; ~-3.29 m NHN) and the upper part (-3.07 m NHN) to 4515–4255 cal BP. For the base of the intercalated peat, the youngest age gained from individual plant remains was preferred over the older bulk sample, as suggested by Hatté and Jull (2007). Regarding the age of the peat top, interpreted as a fen peat, possible incorporation of older $^{14}$C from groundwater has to be considered, leading to a slight age overestimation.

The second peat (starting at ~-5.98 m NHN), as well as the overlying salt marsh documented in VVC16, shows approximately the same age as the underlying sequence of peat and salt marsh. This may suggest that the upper sequence was proximally relocated during a storm event after being ripped off a peat cliff on the mainland coast and deposited in the salt marsh. These drifting peat packages are referred to as '*Dargen*' (Streif, 1990; Behre and Kučan, 1999; van Dijk *et al.*, 2019).

Subsequently, sea-level rise continued and with the south-eastward migrating barrier island the main channel shifted eastwards to the western part of the study area (VVC16 and VVC17). This channel led to subtidal deposition on top of VVC16 but also to erosion and relocation in VVC17. The latter shows >10% of salt-marsh foraminifers within the upper part

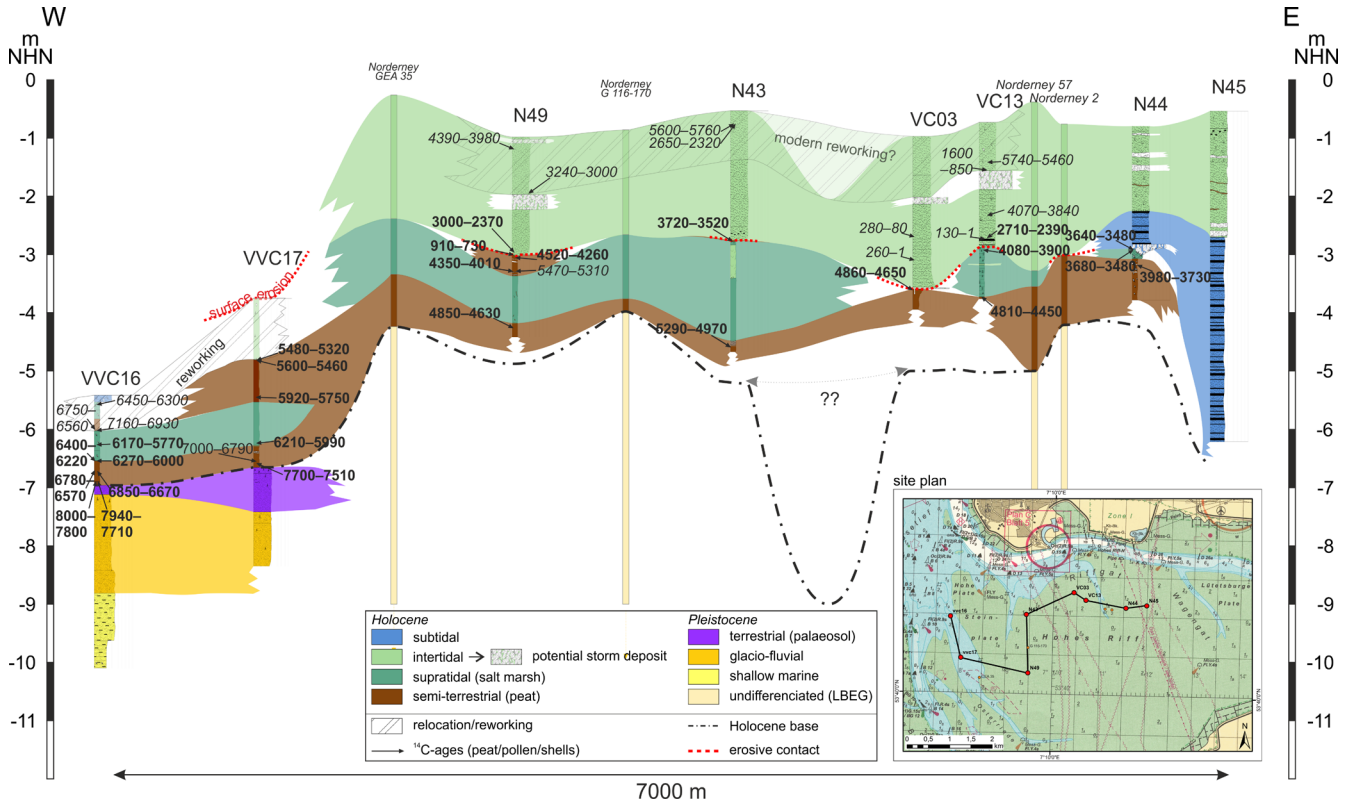


**Figure 5.** Stratigraphic cross section of the cores investigated by Elschner *et al.* (2021), additional WASA and archive core data including radiocarbon ages from peats, bivalve shells and foraminifer tests. Ages written in italics were excluded due to presumed reworking, whereas ages written in bold were deemed reliable. [Color figure can be viewed at wileyonlinelibrary.com]

of the tidal-flat deposits at the top of the core (Bulian *et al.*, 2019). This can only be explained by the introduction of salt-marsh deposits from a fossil layer eroded nearby by channel migration after an initial tidal-flat phase. In the back-barrier area, a tidal flat developed, which in the east was first cut by a smaller channel (N44 and 45) that was subsequently filled. $^{14}$C dating of molluscs and foraminifer shells in four cores (N43, N49, VC03, VC13) suggests a hiatus at the base of the tidal-flat sediments as well as sediment reworking within this unit. The hiatus is well documented in the chronostratigraphy of N49, where the top of the intercalated peat layer is dated to 4515–4255 cal BP, with potential minor overestimation as mentioned earlier, followed by an erosive contact with a burrow of an articulated bivalve (*Barnea candida*) dated to 905–733 cal BP. Reworking is indicated by age data above this hiatus with age inversions in all four cores (Fig. 5) and very young ages derived from molluscs (278–78 and 260–1 cal BP) at depths of -2.7 to -3.1 m NHN (VC03). We expect two different reworking layers, separated by the marker horizon of an undisturbed storm deposit, which can be correlated between all reworking-affected cores, except for N43.

Intense reworking on the tidal flats is mainly connected to dike construction, with first continuous dike systems around AD 1300. It is estimated that up to 50% of the tidal-flat deposits, even more in areas more proximal to the bifurcating channels, are being reworked within 50 years (Trusheim, 1929; Lüders, 1934; Reineck and Siefert, 1980; van der Spek, 1996; Gerdes *et al.*, 2003; Bungenstock *et al.*, 2021). Tidal channels may cut down to more than -20 m to rework substantial amounts of sediment (van der Spek, 1996). The catchment area and the channels themselves are quite stable and channel migration is limited (Bungenstock *et al.*, 2021). For the back-barrier area of Spiekeroog, Tilch (2003) shows that between 1866 and 1935 no significant lateral enlargement of the channel system took place, but there was significant erosional deepening related to dike construction on the mainland and a reduction of the tidal prisms. Over longer time scales, south-eastward migration of the barrier islands intensified tidal dynamics and reworking, as well as episodic storm surges. Tilch (2003) documents vertical erosion of 16 cm for the northern rim of the Janssand, the sandbank between Langeoog and Spiekeroog, during one single summer season (2001), whereas this same amount accumulated in the centre of the sandbank. For more protected sandbanks, seasonal erosion and accumulation rates in the order of 5 cm are reported (Tilch, 2003).

Due to the position of the erosive contact in N49 and VC03 and the reconstructed sloping subsurface structure (Fig. 5), we expect these cores to be influenced by migrating tidal channels. In N43 and VC13, the erosive contact lies higher, which is why reworking after the hiatus is expected to be less intense, at least for the lower part of the tidal-flat deposits. The more recent reworking processes on top of the storm-surge layer may be related to the diurnal tides as well as to the tidal channel between N43 and VC03. The fact that the foraminifer tests in these affected deposits do not show significant signs of relocation (opacity, signs of abrasion) indicates only proximal transport (Hofker, 1977).

# Discussion

## *Evaluation of sample material for TF application*

Samples from non-marine Pleistocene deposits and peat facies were excluded for the application of the RSL TF. Furthermore, deposits with indications for reworking, i.e. most tidal-flat samples, were excluded, since their taphocoenoses may not adequately reflect RSL during deposition. Only the lowest samples from the base of the tidal-flat deposits of VVC17 were included due to the expected lower intensity of reworking implied by the typical shallow-marine (intertidal) foraminifer associations (see *Results and interpretation of the Holocene sediment cores*).

The final TF was applied to 38 (out of originally 139) samples from seven sediment cores. Since Model II of the final TF provides the best vertical error (RMSEP) and correlation ($R^2_{boot}$), only this model was used for the final RSL reconstructions. Therefore, the combined data of foraminifers and ostracods (total = 100%) of each core were integrated. The TF provides the palaeo-elevation of each sample relative to the palaeo-sea level. It was converted to an absolute elevation (m NHN) using the following equation, in order to reflect the palaeo-sea level; the result was plotted against the time (Fig. 6).

$$SL_p = d_s + e_p$$

$SL_p$: palaeo-sea level (m NHN)
$d_s$: depth of fossil sample (m NHN)
$e_p$: palaeo-elevation of fossil sample relative to palaeo-sea level (m)

## *The resulting RSL curve*

The RSL curve and its envelope resulting from applying the TF to the core samples were derived from plotted ages (including their confidence interval of 2σ) and calculated indicative meaning for mean sea level (MSL; including their sample-specific error (Table S2.6 (suppl.)); Fig. 6a). The indicative meaning considers compaction, mean tidal range, and GIA. Fig. 6b shows the final envelope curve including the 2σ uncertainty calculated after the HOLSEA protocol (Khan *et al.*, 2019) in addition. The envelope was drawn connecting the edges of the squares, resulting from the vertical and horizontal error bars, leaving out the older edge where squares overlap. The curve begins during the phase of the transition from faster RSL rise to the decelerated rise. Estimated rates from the graph in the age–depth diagram show a rate of ~0.4 m per century (mean of rates of VVC16 and VVC17) until ~5700 cal BP. However, MAT suggests that the upper two samples of VVC17 as well as the upper sample of VVC16 are not sufficiently reliable (poor modern analogues; Fig. 6), so they should be excluded from the final curve (Fig. 7), leading to a rise of ~0.16 m per century. The first phase is followed by a data gap (no microfaunal data due to peat formation) that correlates with other regional peat records and the deceleration of sea-level rise (Freund and Streif, 2000; Streif, 2004; Bungenstock *et al.*, 2021). The available data between 5000 and ~3700 cal BP indicate a RSL rise of ~0.24 m per century. However, a number of samples show poor modern analogues (e.g. all samples from N49; Fig. 6), which reduces the number of reliable data points with the last reliable data for 4292–3829 cal BP. This does not change the general validity and course of this phase, only the density of reliable data points. Here, the reconstruction shows five visual outliers (one from VC03, two from VVC17, one from VC13 and one from N44). Except for the N44 sample, they represent samples from above the erosive contact. For VVC17, stronger hydrodynamic conditions must have occurred for a certain time before the re-establishment of short-term calmer conditions (indicated by the next sample from this core; Fig. 6). The two outliers from VC03 and VC13 were taken from within a mollusc burrow inside the peat, indicating that the ages of these samples might

 

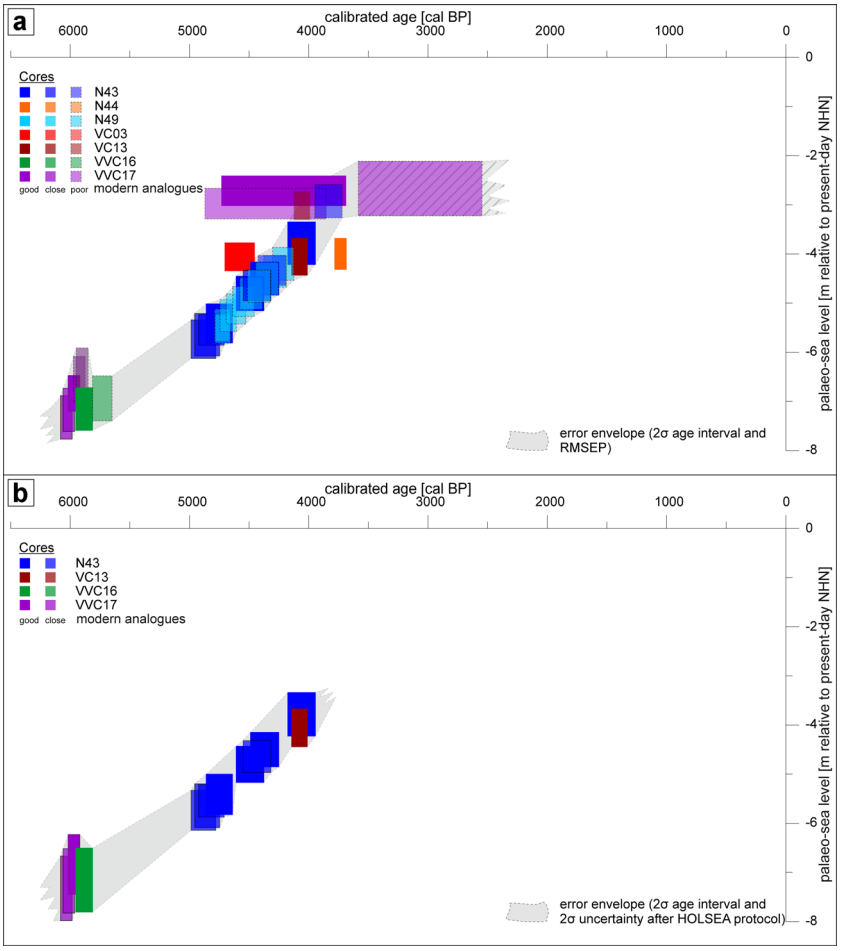


**Figure 6.** Relative sea level (RSL) envelope curve based on the application of the final transfer function (TF) on samples from seven WASA cores in the back-barrier area of Norderney. The curve and its envelope were derived from plotted ages (including their confidence interval, 2σ) and calculated sea levels. Ages are given in calibrated years BP, palaeo-RSL is related to present-day NHN. The quality of the modern analogues is based on the modern analogue technique after Watcham *et al.* (2013). The phase affected by main uncertainties is cross-hatched and visual outlier samples are not included in the envelope. a: error envelope based on 2σ age interval and sample-specific error of the TF (Table S2.6 (suppl)); b: error envelope based on 2σ age interval and 2σ uncertainty following the HOLSEA protocol (suppl. sheet HOLSEA), samples with poor modern analogues and outlier samples excluded. [Color figure can be viewed at wileyonlinelibrary.com]

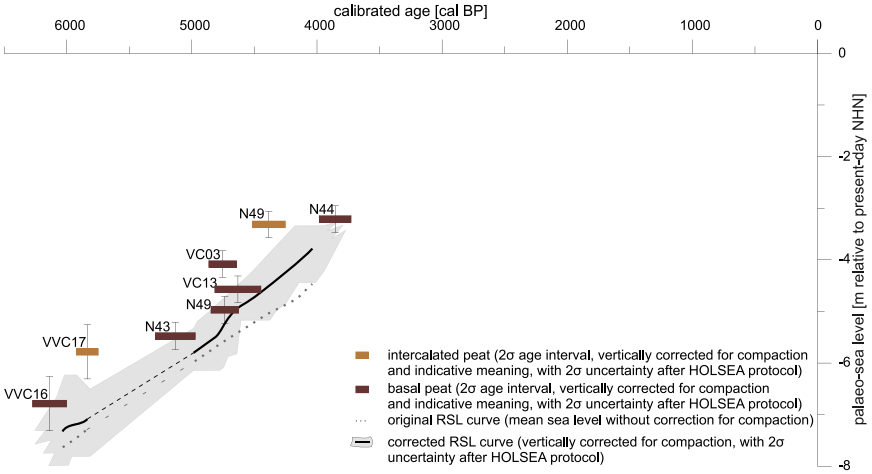


**Figure 7.** Simplified depiction of the decompacted and original relative sea level (RSL) curve for Norderney combined with available sea level-related peat data from the same WASA cores. Ages are given in calibrated years BP and palaeo-RSL, indicative meanings of peat are related to present-day NHN. [Color figure can be viewed at wileyonlinelibrary.com]

be overestimated by the age–depth models. The sample from N44 originates from a salt-marsh layer with a very high organic content (peat), hence, typical calcareous microfauna could have been dissolved (cf. Elschner *et al.*, 2021), possibly biasing the calculation by the TF. Therefore, these samples are not expected to be reliable and were not integrated into the error envelope. The next phase of the curve is characterised by a stagnation between ~3700 and ~2500 cal BP. Since the sample building this phase shows only poor modern analogues (Fig. 6) and age–depth modelling provided a large age error of approximately 1000 years, the third phase is not expected to be reliable and is not considered for the following curve. Changes after ~2500 cal BP cannot be reconstructed due to the exclusion of the reworking-affected tidal-flat samples (see *Evaluation of sample material for TF application*).

Considering the fact that necessary decompaction factors can vary even within one core (Smith *et al.*, 2003, Bungenstock *et al.*, 2021) and the fact that the depth to the Holocene base is not known in cores N43, N49 and VC13, the rate of RSL as depicted by the dataset is subject to some uncertainty. The varying decompaction factors are also a reason for not applying an errors-in-variables integrated Gaussian process (EIV-IGP), which would allow for more detailed rates of RSL change (Cahill *et al.*, 2015, 2016), but would also represent an exponentiation of error estimation and exceed the focus of this article.

In order to fill the gap between ~5700 and ~5000 cal BP and to test the RSL resulting from the TF, we included available peat data related to RSL (basal peat as well as intercalated peat) from the same time span and plotted their reference water level

with the 2σ uncertainty (Table 2 (suppl.)) in the RSL curve (now excluding all TF-based data points with poor modern analogues; Fig. 7). For comparison, Fig. 7 also shows the course of the RSL curve without correction for compaction. It has to be noted that numerical decompaction by calculating the real compaction of the deposits could lead to any decompaction results between the original and the decompacted curve. In general, all peats plot above the TF-based RSL curve and the 2σ uncertainty of most peats overlaps with its error envelope. Only the basal peat of VC03 and the intercalated peat of N49 do not fit the curve. It is possible that both samples are affected by relocation due to their position directly underlying the erosive contact. As mentioned above, these cores are assumed to be influenced by migrating tidal channels. Another possible explanation for the offset of these two data points could be an overestimation of compaction when applying the described decompaction approach. Altogether, the peat data seem more inconsistent than the RSL record of the application of the TF on the same sediment cores.

## *Evaluation of the reconstructed RSL development and comparison with other RSL curves*

In order to assess the validity and trans-regional significance of the decompacted RSL curve, a comparison with existing curves is shown in Figs. 8 and 9. It has to be noted that for the other curves depicted in Fig. 8 neither the standardised calculation of the indicative meaning of peat data following the HOLSEA concept (Hijma and Cohen, 2019; Khan *et al.*, 2019) nor a TF for microfauna data has been applied. Nevertheless, a general tendency of MSL curves along the southern North Sea coast can be described.

Considering the differences to Belgium and Zeeland (Denys and Baeteman, 1995; Kiden, 1995; Vink *et al.*, 2007), the present curve shows a generally lower course but approximates to the Belgian curve in time and shows a smaller error envelope in the second phase. During the first phase, the present reconstruction lies lower than the ones from Belgium and Zeeland, whereas in the second phase (~5000–3700 cal BP), the difference becomes smaller towards the end of the phase. The general deviation could be explained by northward increasing glacial isostatic subsidence due to the position relative to the north-west–east-south-east orientated glacial forebulge (Kiden *et al.*, 2002; Meijles *et al.*, 2018). The overall decreasing differences may relate to slowly decreasing subsidence rates over time (cf. Kiden *et al.*, 2002; Vink *et al.*, 2007).

The differences between the present curve and curves from the central and western Netherlands (van de Plassche *et al.*, 2005; Hijma and Cohen, 2010, 2019) as well as from the Dutch Wadden Sea (Meijles *et al.*, 2018) are smaller, but also decreasing with time. The error envelope of the present curve is similar to the one from the central Netherlands (van de Plassche *et al.*, 2005) in the second phase, but seems larger for the rest of the curve. Concerning the curve for the Dutch Wadden Sea (Meijles *et al.*, 2018), the error envelope of the second phase of our TF-based curve is generally smaller. The general trend of the present curve is most similar to the compaction-resistant curve from the Flevo area that only uses the base of basal peats as sea-level index points (SLIPs) (van de Plassche *et al.*, 2005). The elevation differences between the TF-based curve and all three mentioned curves could partly be explained by different concepts of depicting MSL but, nevertheless, for the main part by the different GIA rates and, to some extent, tectonics (Meijles *et al.*, 2018). The approximation of the curves during the second phase may again show the decreasing subsidence rates over time (cf. Kiden *et al.*, 2002; Vink *et al.*, 2007).

The present curve shows overlaps with the one for north-west Germany (Vink *et al.*, 2007), mainly concerning their error envelopes, even though it is generally lower. The curve for north-west Germany is based on selected data previously published by Behre (2003, 2007) which led to a smoother curve than the original one. The error envelope of the complete TF-based curve is smaller than that of the curve for north-west Germany. Taking a closer look at the differences during the first phase, these data (top of basal peats and base of intercalated peat) are definitely influenced by compaction (Vink *et al.*, 2007), whereas our curve includes a decompaction approach. Furthermore, the six data points originate from a very large section of the German coast, reaching from Emden, close to the Dollart Bay, over Hooksiel and Wilhelmshaven (Jade Bay) to the 'Land Wursten' region (>10 km south of Cuxhaven) and none are located near Norderney, implying an interregional significance of the different SLIPs (Bungenstock and Weerts, 2010, 2012). Considering different local effects (mean tidal range, GIA), our curve is therefore associated with a higher significance, at least for the present study area, even if the steep trend of the first phase remains uncertain due to the poor modern analogues. Looking at the database of Behre (2003) for the time of the second phase of the present curve, a similar pattern becomes apparent concerning the compaction-prone database (top and base of upper peats and intercalated peat). The Behre dataset is not as regionally widespread for this phase, possibly representing a significance for the area around the Jade Bay, but not for the tidal basin of Norderney.

The present curve cannot be connected to the curve from the West Frisian Islands for the last 2000 years (De Groot *et al.*, 1996) due to the exclusion of the uppermost VVC17 sample with poor analogues and of the reworking-affected tidal-flat samples.

Comparing the TF-based RSL data with RSL curves applying the standardised calculation of the indicative meaning of peat data following the HOLSEA concept leads to smaller deviations (Fig. 9). A new peat-based curve from the East Frisian Island of Langeoog (~10 km east of Norderney, Bungenstock *et al.*, 2021) lies only slightly above the present TF curve with both curves showing overlapping error envelopes. Differences may be due to the nature of the dataset of Bungenstock *et al.* (2021) (tidal-flat sediments vs. peat data) but also due to the

**Table 2.** Overview of the indicative meaning for the fen peats plotted in the age–depth diagram in Fig. 7. For the peat characterisation, see Table 1.

| Sample type | Evidence | Reference water level (RWL) when selected as sea-level index point with mean high water (MHW) = 1.2 m for Norderney (BSH, 2018) | Reference water level (RWL) when not selected as sea-level index point = ground water level (GWL) | Indicative range |
|---|---|---|---|---|
| Fen peat | The average water depth is set at 0.3 m and the indicative range at 0.2 m (Hijma and Cohen, 2019) | MHW -0.3 m | GWL -0.3 m | RWL ± 0.2 m |

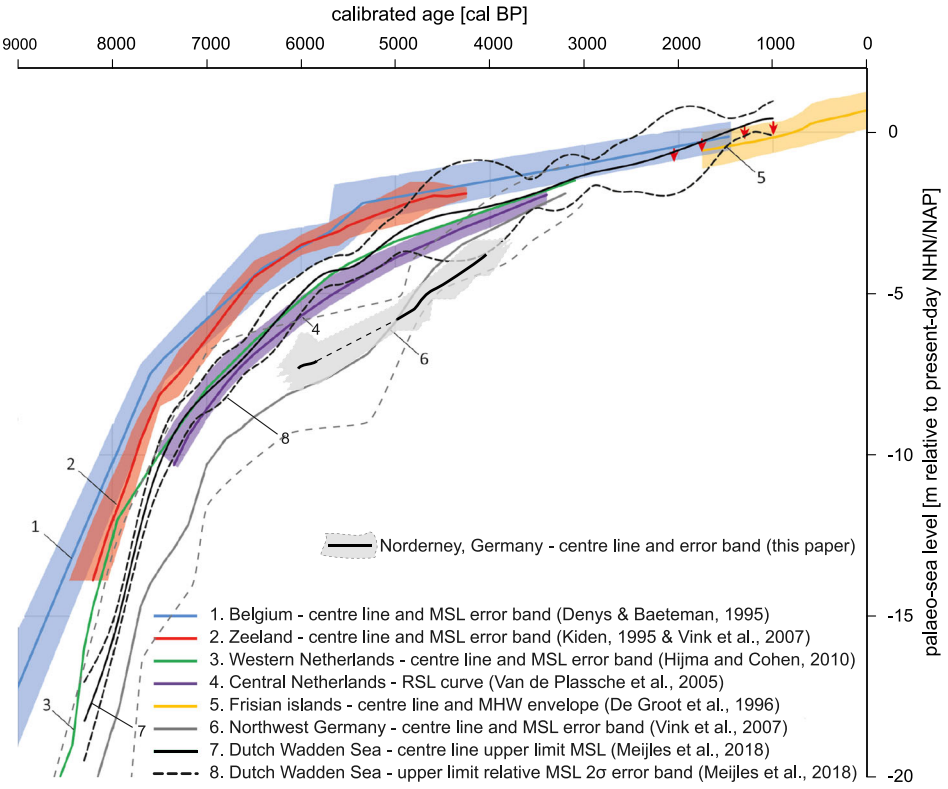


**Figure 8.** Compilation of RSL curves established along the North Sea coast of Belgium, the Netherlands and Germany. Our data are plotted on top of the existing curves in order to detect differences and similarities. Design modified after Meijles *et al.* (2018). [Color figure can be viewed at wileyonlinelibrary.com]

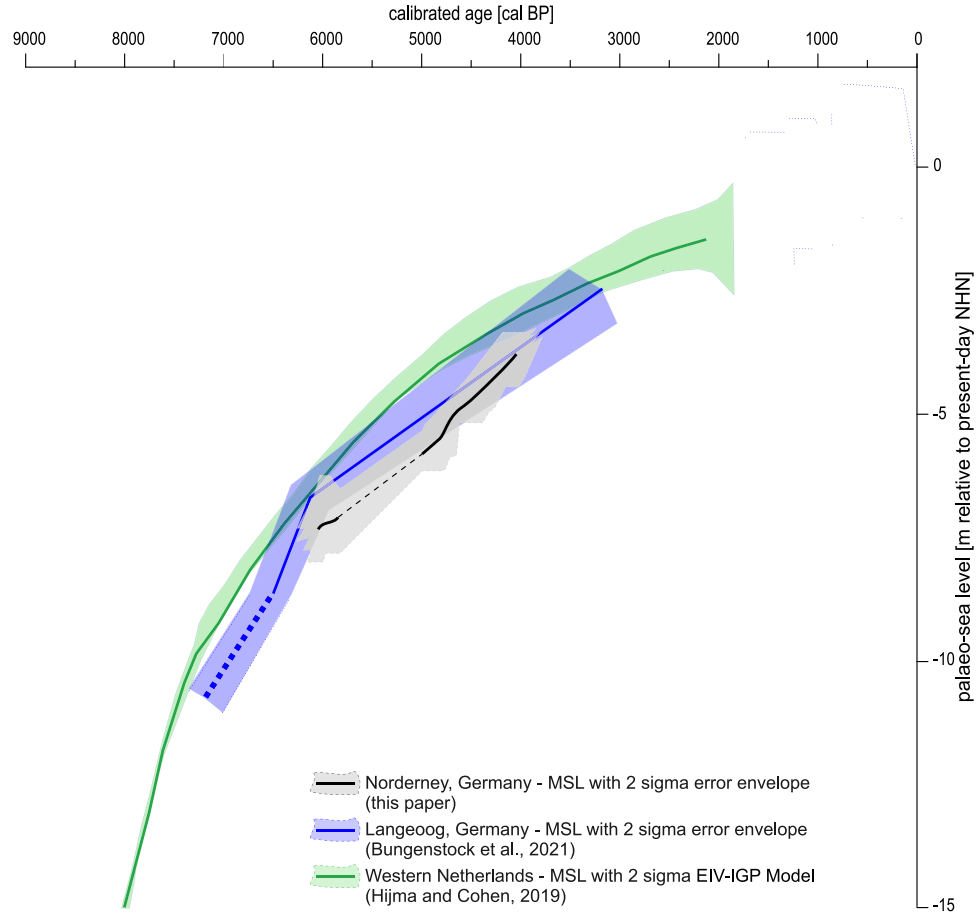


**Figure 9.** Compilation of our relative sea level (RSL) data, the revised RSL data of Hijma and Cohen (2019) now applying the indicative-meaning concept, and new data from the East Frisian Island of Langeoog recently published by Bungenstock *et al.* (2021). [Color figure can be viewed at wileyonlinelibrary.com]

applied decompaction approach leading to a higher rate in RSL rise in the second phase of the TF curve. A possible underestimation of the compaction in the lower parts of N43 due to the unknown depth of the Holocene base could have pretended a higher rate in that phase, also explaining the larger difference between the two curves around ~5000 cal BP. Another possible reason could be the underestimation of the indicative meaning of the peats by Bungenstock *et al.* (2021). Hence, most likely, no real offset exists between the two tidal basins. However, the error envelope of the TF curve in the second phase is much smaller than the one of the peat-based Langeoog curve (Bungenstock *et al.*, 2021).

Comparing the present curve with the more recent RSL curve for the western Netherlands (Hijma and Cohen, 2019) (Fig. 9) shows that the two curves lie much closer when applying the indicative-meaning concept, which was not the case for the predecessor curve (Hijma and Cohen, 2010) (Fig. 8). The tendency is still the same, but the differences are smaller: in the first phase, the difference decreased from ~2 m to ~1 m and in the second phase it decreased from ~2.4–1.2 m to ~1.6–0.6 m. However, the decreasing difference of the second phase could be weakened when considering a possible underestimation of compaction in the lower parts of N43 (beginning of the second phase ~5000–4500 cal BP) due to the unknown depth of the Holocene base. In that case, a mainly parallel trend of both curves can be assumed.

## Conclusion and outlook

The inclusion of additional samples from the vicinity of the surface transect (Scheder *et al.*, 2019) helps to improve the performance of the preliminary TF for RSL. The vertical error of the common TF model, using only dead foraminifers, could be improved by ±8 cm by including dead ostracods. The final TF provides an $R^2_{boot}$ of 0.89 and a vertical error of 29.7 cm, accounting for ~11% of the tidal range of Spiekeroog (BSH, 2018). The overall error range lies at ~1 m.

The Holocene stratigraphic sequence of the back-barrier area of Norderney starts with Pleistocene deposits, which are overlain by the basal peat resulting from rising groundwater levels associated with the early to mid-Holocene trangression (Streif, 2004; Bungenstock and Schäfer, 2009). Peat growth started around 8000–7500 cal BP in the west and expanded further east. A salt-marsh layer on top of the basal peat indicates increasing marine influence. In general, peat and salt-marsh formation continue to the east with a delay, following the RSL rise at the back of the gradually forming barrier island. The tidal-flat record starts with a massive hiatus (~1000–3300 years), and $^{14}C$ ages suggest reworking throughout the study area, which is mainly connected to the change in hydrodynamics associated with dike construction (Trusheim, 1929; Lüders, 1934; Reineck and Siefert, 1980; van der Spek, 1996).

The first Holocene RSL curve resulting from the application of a TF in the southern North Sea region shows a deceleration in sea-level rise between 6000 and 5000 cal BP. Due to the low reliability of the tidal-flat deposits, poor modern analogues and a large age error of the data, we are not able to reliably reconstruct RSL changes younger than ~4000 years. Nevertheless, the RSL curve provides a smaller error envelope than many of the peat-based curves (Denys and Baeteman, 1995; Vink *et al.*, 2007; Meijles *et al.*, 2018) and represents a more continuous record. The applied decompaction approach appears to be robust for the samples applied in the study area, although the course of the curve may suggest a partial underestimation of compaction. This confirms the importance of locally different compaction rates. Besides this, a local comparison to a new peat-based curve for Langeoog (Bungenstock *et al.*, 2021) shows a good agreement of both curves and no considerable offset.

In general, the reworking that influences the reliability of the tidal-flat samples can only be circumvented by investigating sediment archives from inner-dike locations providing younger salt-marsh deposits. Along a transect perpendicular to the coastline, these could also capture fossil tidal-flat deposits that have not been influenced by intense reworking (Karle *et al.*, 2021). A correction for tidal changes, by adjusting the TF based on palaeotide models, remains a goal for future studies.

*Acknowledgements.* The research reported here is part of the WASA project (*The Wadden Sea as an archive of landscape evolution, climate change and settlement history: exploration – analysis – predictive modelling*), funded by the 'Niedersächsisches Vorab' of the VolkswagenStiftung within the funding initiative 'Küsten und Meeresforschung in Niedersachsen' of the Ministry for Science and Culture of Lower Saxony, Germany (project VW ZN3197). We especially thank the colleagues and students from the Niedersächsischer Landesbetrieb für Wasserwirtschaft, Küsten- und Naturschutz (NLWKN), Senckenberg am Meer and the Lower Saxony Institute for Historical Coastal Research, who took the cores. Samples from the 11 transect stations were collected within the research project BEFmate (BiodiversityEcosystemFunctioning across marine and terrestrial ecosystems) under project number ZN2930. Oxygen and TOC data were provided by Jennifer Schmitt (ICBM – Institute for Chemistry and Biology of the Marine Environment) and Gesine Lange (University of Oldenburg) in the frame of the BEFmate project. Dirk Enters (Lower Saxony Institute for Historical Coastal Research), Alexander Bartholomä and Ruggero Capperucci (Senckenberg am Meer) are acknowledged for macroscopic core descriptions, as well as Annastasia Elschner (University Bonn), Shirin Nurshan Rahman (Senckenberg am Meer) and Anika Symanczyk (University of Cologne) for laboratory assistance. Furthermore, we gratefully acknowledge Torsten Janßen (Senckenberg am Meer) for extensive organisational work concerning radiocarbon dating. The EasyCopy company is acknowledged for providing the core-drawing software (EasyCore). The Landesamt für Bergbau, Geologie und Energie (LBEG), Hannover, is thanked for providing the archive core data. Helpful suggestions of two anonymous reviewers greatly improved this paper. Open Access funding enabled and organized by Projekt DEAL.

### *Data availability statement*

The data that support the findings of this study are available in the supplementary material of this article.

## Supporting information

Additional supporting information can be found in the online version of this article.

S1. Applied methods (outside main focus of the paper). S1.1 Laboratory analyses – Core drillings. S1.2 Data processing – Core drillings. S2. Results – modern samples and core drillings. S2.1 Microfauna – taxa and ecological information. Figure S2.1: SEM images of frequently documented foraminifer and ostracod species. S2.2 Results of modern samples. Table S2.1: List of foraminifers. Table S2.2: Total organic carbon values. Table S2.3: Replicated oxygen values. Table S2.4: Foraminifer- and ostracod counts of the combined dataset. Figure S2.2: DCA biplot showing the two most relevant axes. S2.3 Sedimentological, geochemical and microfaunal results of core drillings. Table S2.5: Logistical core data of the investigated core drillings as well as the archive core data. Figure S2.3: Sedimentological, geochemical and microfaunal results as well as facies interpretation of VVC16. Figure S2.4: Sedimentological, geochemical and microfaunal results as well as facies interpretation of N49. Figure S2.5: Sedimentological, geochemical and microfaunal results as well as

 

facies interpretation of N43. Figure S2.6: Sedimentological, geochemical and microfaunal results as well as facies interpretation of VC03. Figure S2.7: Sedimentological, geochemical and microfaunal results as well as facies interpretation of VC13. Figure S2.8: Sedimentological, geochemical and microfaunal results as well as facies interpretation of N44. Figure S2.9: Sedimentological, geochemical and microfaunal results as well as facies interpretation of N45. S2.4 Application of the transfer function. Table S2.5: Transfer function derived water depth, palaeo-sea level and modelled age for each sample used for RSL reconstruction. Supplementary Excel sheet: Scheder_et_al_2021_HOLSEA.

## References


Athersuch J, Horne DJ, Whittaker JE. 1989. *Marine and brackish water ostracods (superfamilies Cypridacea and Cytheracea): keys and notes for the identification of the species*. Brill Archive, Leiden.

Baeteman C. 1999. The Holocene depositional history of the IJzer palaeovalley (Western Belgian coastal plain) with reference to the factors controlling the formation of intercalated peat beds. *Geologica Belgica* **2**: 39–72.

Baeteman C, Waller M, Kiden P. 2011. Reconstructing middle to late Holocene sea-level change: A methodological review with particular reference to 'A new Holocene sea-level curve for the southern North Sea' presented by K.-E. Behre. *Boreas* **40**: 557–572.

Bakker JP. 2014. *Ecology of Salt Marshes: 40 Years of Research in the Wadden Sea*. Wadden Academy: Leeuwarden.

Barlow NLM, Shennan I, Long AJ *et al*. 2013. Salt marshes as late Holocene tide gauges. *Global and Planetary Change* **106**: 90–110.

Beck HE, Zimmermann NE, McVicar TR *et al*. 2018. Present and future Köppen-Geiger climate classification maps at 1-km resolution. *Scientific Data* **5**: 180214.

Behre K-E. 2003. Eine neue Meeresspiegelkurve für die südliche Nordsee. *Probleme der Küstenforschung im südlichen Nordseegebiet* **28**: 9–63.

Behre K-E. 2007. A new Holocene sea-level curve for the southern North Sea. *Boreas* **36**: 82–102.

Behre K-E, Kučan D. 1999. Neue Untersuchungen am Außendeichsmoor bei Sehestedt am Jadebusen. *Probleme der Küstenforschung im südlichen Nordseegebiet* **26**: 35–64.

Bird MI, Fifield LK, Chua S *et al*. 2004. Calculating Sediment Compaction for Radiocarbon Dating of Intertidal Sediments. *Radiocarbon* **46**: 421–435.

Birks HJB. 1995. Quantitative palaeoenvironmental reconstructions. In *Statistical Modelling of Quaternary Science Data*, Maddy D, Brew JS (eds.). Quaternary Research Association: Cambridge; 161–254.

Bittmann F. 2019. Das Wattenmeer als Archiv zur Landschaftsentwicklung, Klimaänderung und Siedlungsgeschichte. *Nachrichten des Marschenrats zur Förderung der Forschung im Küstengebiet der Nordsee* **56**: 25–27.

Blaauw M, Christen A 2019. rbacon: Age-Depth Modelling using Bayesian Statistics. R package version 2.3.9.1. https://CRAN.R-project.org/package=rbacon

BSH (Bundesamt für Seeschifffahrt und Hydrographie). 2018. *Gezeitenkalender 2019: Hoch- und Niedrigwasserzeiten für die Deutsche Bucht und deren Flussgebiete*. Bundesamt für Seeschifffahrt und Hydrographie: Hamburg.

Bulian F, Enters D, Schlütz F *et al*. 2019. Multi-proxy reconstruction of Holocene paleoenvironments from a sediment core retrieved from the Wadden Sea near Norderney, East Frisia, Germany. *Estuarine, Coastal and Shelf Science* **225**: 106251.

Bungenstock F, Schäfer A. 2009. The Holocene relative sea-level curve for the tidal basin of the barrier island Langeoog, German Bight, Southern North Sea. *Global and Planetary Change* **66**: 34–51.

Bungenstock F, Weerts HJT. 2010. The high-resolution Holocene sea-level curve for Northwest Germany: global signals, local effects or data-artefacts? *International Journal of Earth Sciences* **99**: 1687–1706.

Bungenstock F, Weerts HJT. 2012. Holocene relative sea-level curves for the German North sea coast. *International Journal of Earth Sciences* **101**: 1083–1090.

Bungenstock F, Freund H, Bartholomä A. 2021. Holocene relative sea-level data for the East Frisian barrier coast, NW Germany, southern North Sea. *Netherlands Journal of Geosciences* **100**: 00. (In press).

Cahill N, Kemp AC, Horton BP *et al*. 2015. Modeling sea-level change using errors-in-variables integrated Gaussian processes. *The Annals of Applied Statistics* **9**: 547–571.

Cahill N, Kemp AC, Horton BP *et al*. 2016. A Bayesian hierarchical model for reconstructing relative sea level: from raw data to rates of change. *Climate of the Past* **12**: 525–542.

Davis JC. 1986. *Statistics and Data Analysis in Geology*. 2nd ed. John Wiley & Sons: New York.

De Groot TAM, Westerhoff WE, Bosch JHA. 1996. Sea-level rise during the last 2000 years as recorded on the Frisian Islands (the Netherlands). *Mededelingen Rijks Geologische Dienst* **57**: 69–78.

Denys L, Baeteman C. 1995. Holocene evolution of relative sea level and local mean high water spring tides in Belgium — a first assessment. *Marine Geology* **124**: 1–19.

Edwards RJ, Wright A. 2015. Foraminifera. In *Handbook of Sea-Level Research*, Shennan I, Long AJ, Horton BP (eds.). John Wiley & Sons: Chichester; 191–217.

Elschner A, Scheder J, Enters D *et al*. 2021. Microfauna- and sedimentology-based facies analysis for palaeo-landscape reconstruction in the back-barrier of Norderney (NW Germany). *Netherlands Journal of Geosciences* **100**: e4.

Enters D, Haynert K, Wehrmann A *et al*. 2021. A new ΔR value for the southern North Sea and its application in coastal research. *Netherlands Journal of Geosciences* **100**: e1.

Flemming BW 2002. Effects of Climate and Human Interventions on the Evolution of the Wadden Sea Depositional System (Southern North Sea). In *Climate Development and History of the North Atlantic Realm*, Wefer G, Berger WH, Behre K-E *et al*. (eds.). Springer: Berlin, Heidelberg; 399–413.

Flemming BW, Davis Jr., RA. 1994. Holocene evolution, morphodynamics and sedimentology of the Spiekeroog barrier island system (southern North Sea). *Senckenbergiana maritima* **24**: 117–155.

Flemming BW, Ziegler K. 1995. High-resolution grain size distribution patterns and textural trends in the backbarrier environment of Spiekeroog Island (southern North Sea). *Senckenbergiana maritima* **26**: 1–24.

Frenzel P, Tech T, Bartholdy J. 2005. Checklist and annotated bibliography of Recent Foraminiferida from the German Baltic Sea coast. *Studia Geologica Polonica* **124**: 67–86.

Frenzel P, Keyser D, Viehberg FA. 2010. An illustrated key and (palaeo)ecological primer for Postglacial to Recent Ostracoda (Crustacea) of the Baltic Sea. *Boreas* **39**: 567–575.

Freund H, Streif H. 2000. Natürliche Pegelmarken für Meeresspiegelschwankungen der letzten 2000 Jahre im Bereich der Insel Juist. *Petermanns Geographische Mitteilungen* **143**: 34–45.

Gerdes G, Petzelberger BEM, Scholz-Böttcher BM *et al*. 2003. The record of climatic change in the geological archives of shallow marine, coastal, and adjacent lowland areas of Northern Germany. *Quaternary Science Reviews* **22**: 101–124.

Hammer Ø, Harper DAT, Ryan PD. 2001. Past: Paleontological statistics software package for education and data analysis. *Palaeontologia Electronica* **4**: article 4.

Harper DAT (ed). 1999. *Numerical Palaeobiology. Computer-Based Modelling and Analysis of Fossils and their Distributions*. John Wiley & Sons: Chichester.

Hatté C, Jull AJT. 2007. Plant Macrofossils. In *Encyclopedia of Quaternary Science*, Scott AE (ed.). Elsevier: Oxford; 2958–2965.

Hesemann M. 2015. The foraminifera.eu database: concept and status. *Palaeontologia Electronica* **18.3.48A**: 1–14.

Hijma MP, Cohen KM. 2010. Timing and magnitude of the sea-level jump preluding the 8200 yr event. *Geology* **38**: 275–278.

Hijma MP, Cohen KM. 2019. Holocene sea-level database for the Rhine-Meuse Delta, The Netherlands: Implications for the pre-8.2 ka sea-level jump. *Quaternary Science Reviews* **214**: 68–86.

Hijma MP, Engelhart SE, Törnqvist TE *et al*. 2015. A protocol for a geological sea-level database. In *Handbook of Sea-Level Research*, Shennan I, Long AJ, Horton BP (eds.). John Wiley & Sons: Chichester; 536–554.

Hofker J. 1977. The foraminifera of Dutch tidal flats and salt marshes. Netherlands. *Journal of Sea Research* **11**: 223–296.


 

Juggins S 2007. *C2 Version 1.5: software for ecological and palaeoecological data analysis and visualisation*. University of Newcastle, Newcastle upon Tyne.

Karle M, Bungenstock F, Wehrmann A. 2021. Holocene coastal landscape development in response to rising sea level in the Central Wadden Sea coastal region. *Netherlands Journal of Geosciences* **100**: e12.

Kemp AC, Telford RJ. 2015. Transfer functions. In *Handbook of Sea-Level Research,*. Shennan I, Long AJ, Horton BP (eds.). John Wiley & Sons: Chichester; 470–499.

Kemp AC, Horton BP, Vann DR *et al*. 2012. Quantitative vertical zonation of salt-marsh foraminifera for reconstructing former sea level; an example from New Jersey, USA. *Quaternary Science Reviews* **54**: 26–39.

Khan NS, Horton BP, Engelhart S *et al*. 2019. Inception of a global atlas of sea levels since the Last Glacial Maximum. *Quaternary Science Reviews* **220**: 359–371.

Kiden P. 1995. Holocene relative sea-level change and crustal movement in the southwestern Netherlands. *Marine Geology* **124**: 21–41.

Kiden P, Denys L, Johnston P. 2002. Late Quaternary sea-level change and isostatic and tectonic land movements along the Belgian–Dutch North Sea coast: geological data and model results. *Journal of Quaternary Science* **17**: 535–546.

Kottek M, Grieser J, Beck C *et al*. 2006. World map of the Köppen-Geiger climate classification updated. *Meteorologische Zeitschrift* **15**: 259–263.

Lange G, Haynert K, Dinter T *et al*. 2018. Adaptation of benthic invertebrates to food sources along marine-terrestrial boundaries as indicated by carbon and nitrogen stable isotopes. *Journal of Sea Research* **131**: 12–21.

Last WM, Smol JP. 2001. *Tracking Environmental Change Using Lake Sediments. Volume 2: Physical and Geochemical Methods*. Kluwer Academic Publishers: Dordrecht.

Leorri E, Gehrels WR, Horton BP *et al*. 2010. Distribution of foraminifera in salt marshes along the Atlantic coast of SW Europe: Tools to reconstruct past sea-level variations. *Quaternary International* **221**: 104–115.

Lepš J, Šmilauer P. 2003. *Multivariate analysis of ecological data Using CANOCO*. Cambridge University Press: New York.

Long AJ, Waller MP, Stupples P. 2006. Driving mechanisms of coastal change: Peat compaction and the destruction of late Holocene coastal wetlands. *Marine Geology* **225**: 63–84.

Lüders K. 1934. Über das Wandern der Priele. *Abhandlungen des Naturwissenschaftlichen Vereins zu Bremen* **29**: 19–32.

Lutze GF, Altenbach AV. 1991. Technik und Signifikanz der Lebendfärbung benthischer Foraminiferen in Bengalrot. *Geologisches Jahrbuch* **128**: 251–265.

Meijles EW, Kiden P, Streurman H-J *et al*. 2018. Holocene relative mean sea-level changes in the Wadden Sea area, northern Netherlands. *Journal of Quaternary Science* **33**: 905–923.

Milker Y, Weinkauf MFG, Titschack J *et al*. 2017. Testing the applicability of a benthic foraminiferal-based transfer function for the reconstruction of paleowater depth changes in Rhodes (Greece) during the early Pleistocene. *PLoS ONE* **12**: 0188447.

Müller-Navarra K, Milker Y, Schmiedl G. 2016. Natural and anthropogenic influence on the distribution of salt marsh foraminifera in the Bay of Tümlau, German North Sea. *Journal of Foraminiferal Research* **46**: 61–74.

Murray JW. 2000. The enigma of the continued use of total assemblages in ecological studies of benthic Foraminifera. *Journal of Foraminiferal Research* **30**: 244–245.

Murray JW. 2006. *Ecology and Applications of Benthic Foraminifera*. Cambridge University Press: Cambridge.

Pizzuto JE, Schwendt AE. 1997. Mathematical modeling of auto-compaction of a Holocene transgressive valley-fill deposit, Wolfe Glade, Delaware. *Geology* **25**: 57–60.

Preuß H, Vinken R, Vorr H-H. 1991. *Symbolschlüssel Geologie*. 3rd ed. Niedersächsisches Landesamt für Bodenforschung und Bundesanstalt für Geowissenschaften und Rohstoffe: Hannover.

Rahman SN 2018. *Distribution of salt marsh foraminifera*. Universität Oldenburg.

Rahmstorf S. 2017. Rising hazard of storm-surge flooding. *Proceedings of the National Academy of Sciences of the United States of America* **114**: 11806–11808.

Reimer PJ, Bard E, Bayliss A *et al*. 2013. IntCal13 and Marine13 Radiocarbon Age Calibration Curves 0–50,000 Years cal BP. *Radiocarbon* **55**: 1869–1887.

Reineck H-E, Siefert W. 1980. Faktoren der Schlickbildung im Sahlenburger und Neuwerker Watt. *Die Küste* **35**: 26–51.

Scheder J, Frenzel P, Bungenstock F *et al*. 2019. Vertical and lateral distribution of Foraminifera and Ostracoda in the East Frisian Wadden Sea – developing a transfer function for relative sea-level change. *Geologica Belgica* **22**: 99–110.

Smith DE, Wells JM, Mighall TM *et al*. 2003. Holocene relative sea levels and coastal changes in the lower Cree valley and estuary, SW Scotland, U.K. *Transactions of the Royal Society of Edinburgh, Earth Sciences* **93**: 301–331.

Streif H. 1990. *Das ostfriesische Küstengebiet. Nordsee, Inseln, Watten und Marschen. Sammlung Geologischer Führer 57*. 2nd ed. Gebrüder Bornträger: Berlin.

Streif H. 2004. Sedimentary record of Pleistocene and Holocene marine inundations along the North Sea coast of Lower Saxony, Germany. *Quaternary International* **112**: 3–28.

Tilch E. 2003. Oszillation von Wattflächen und deren fossiles Erhaltungspotential (Spiekerooger Rückseitenwatt, Südliche Nordsee). Berichte, Fachbereich Geowissenschaften, Universität Bremen, Bremen.

Trusheim F. 1929. Zur Bildungsgeschwindigkeit geschichteter Sedimente im Wattenmeer, besonders solcher mit schräger Parallelschichtung. *Senckenbergiana* **11**: 47–56.

van Asselen S. 2011. The contribution of peat compaction to total basin subsidence: implications for the provision of accommodation space in organic-rich deltas. *Basin Research* **23**: 239–255.

van de Plassche O. 1986. *Sea-level research: a manual for the collection and evaluation of data*. Springer: Netherlands.

van de Plassche O, Bohncke SJP, Makaske B *et al*. 2005. Water-level changes in the Flevo area, central Netherlands (5300–1500 BC): implications for relative mean sea-level rise in the Western Netherlands. *Quaternary International* **133–134**: 77–93.

van de Plassche O, Makaske B, Hoek WZ *et al*. 2010. Mid-Holocene water-level changes in the lower Rhine-Meuse delta (western Netherlands): implications for the reconstruction of relative mean sea-level rise, palaeoriver-gradients and coastal evolution. *Netherlands Journal of Geosciences* **89**: 3–20.

van der Spek A. 1996. Holocene depositional sequences in the Dutch Wadden Sea south of the island of Ameland. *Mededelingen Rijks Geologische Dienst* **57**: 41–68.

van Dijk G, Fritz C, Straathof N *et al*. 2019. Biogeochemical characteristics of the last floating coastal bog remnant in Europe, the Sehestedt Bog. *Wetlands* **39**: 227–238.

van Wijnen HJ, Bakker JP. 2001. Long-term surface elevation change in salt marshes: A prediction of marsh response to future sea-level rise. *Estuarine, Coastal and Shelf Science* **52**: 381–390.

Vink A, Steffen H, Reinhardt L *et al*. 2007. Holocene relative sea-level change, isostatic subsidence and the radial viscosity structure of the mantle of northwest Europe (Belgium, the Netherlands, Germany, southern North Sea). *Quaternary Science Reviews* **26**: 3249–3275.

Walton WR. 1952. Techniques for recognition of living Foraminifera. *Contribution Cushman Foundation of Foraminiferal Research* **3**: 56–60.

Watcham EP, Shennan I, Barlow NLM. 2013. Scale considerations in using diatoms as indicators of sea-level change: Lessons from Alaska. *Journal of Quaternary Science* **28**: 165–179.

Weerts HJT. 2013. Holocene sea-level change, sedimentation, coastal change and palaeogeography in the southern North Sea lowlands. A 2012 geological literature overview. In Landscapes or Seascapes? The History of the Coastal Environment in the North Sea Area Reconsidered, Thoen E, Borger GJ, de Kraker AMJ, *et al.* (eds.). CORN Publication Series, 13. Brepols Publishers: Turnhout; 145–173.

Weisse R, von Storch H, Niemeyer HD *et al*. 2012. Changing North Sea storm surge climate: An increasing hazard? *Ocean and Coastal Management* **68**: 58–68.

Woodroffe CD, Murray-Wallace CV. 2012. Sea-level rise and coastal change: the past as a guide to the future. *Quaternary Science Reviews* **54**: 4–11.

Wright AJ, Edwards RJ, van de Plassche O. 2011. Reassessing transfer-function performance in sea-level reconstruction based on benthic salt-marsh foraminifera from the Atlantic coast of NE North America. *Marine Micropaleontology* **81**: 43–62.

 